Supplement of The Cryosphere, 19, 1717–1724, 2025
https://doi.org/10.5194/tc-19-1717-2025-supplement


The Cryosphere Open Access EGU

*Supplement of*

# Brief communication: Storstrømmen Glacier, northeastern Greenland, primed for end-of-decade surge

**Jonas K. Andersen et al.**

*Correspondence to:* Jonas K. Andersen (joka@ign.ku.dk)

## Supplementary Figures

**Figure S1** - Example of grounding line mapping

**Figure S2** - Evidence of flow acceleration and uplift following drainage events

**Figure S3** - Evidence of subsidence following drainage events

**Figure S4** - Sentinel-1 amplitude images related to Storstrømmen drainage events

**Figure S5** - ArcticDEM elevation difference maps showing evidence of lake drainages

**Figure S6** - Documentation of additional transient dynamic events in upstream Storstrømmen (December 2018 and May 2019)

**Figure S7** - Documentation of transient dynamic event in upstream L. Bistrup

**Figure S8** - Sentinel-1 amplitude images related to the L. Bistrup drainage event

**Figure S9** - Grounding line location time series for L. Bistrup

## Supplementary Tables

**Table S1** - Acquisition dates of reference Sentinel-1 image pairs

## References

Chudley, T. and Howat, I.: (2024). pDEMtools: conveniently search, download, and process ArcticDEM and REMA products. Journal of Open Source Software, 9(102), 7149, https://doi.org/10.21105/joss.07149

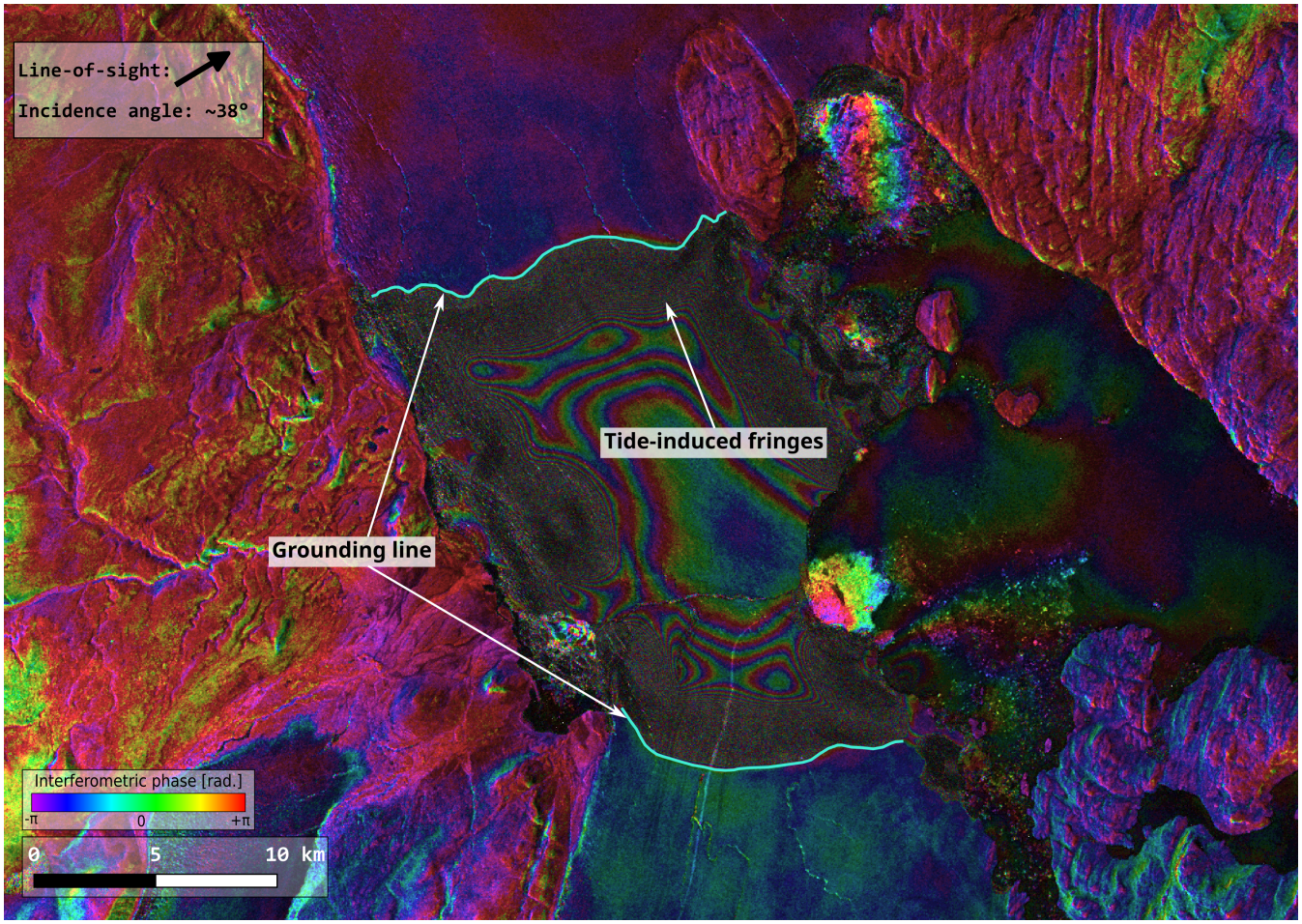


**Figure S1.** Sentinel-1 double-difference interferogram exemplifying the mapping of grounding lines for Storstrømmen (top) and L. Bistrup (bottom). The phase of the double-difference interferogram is sensitive to changes in the displacement field between the two interferograms (in this case spanning the temporal baselines 10th - 16th April 2018 and 16th - 22nd April 2018) in the radar line-of-sight, and a denser fringe pattern indicates a larger displacement change. Assuming no changes in horizontal ice flow between the two interferograms, the dense fringe pattern observed here is caused by a difference in the tide amplitude between the two interferograms, which leads to a difference in vertical uplift. The upstream limit of these tidally induced fringes is interpreted as a proxy for the glacier grounding line.

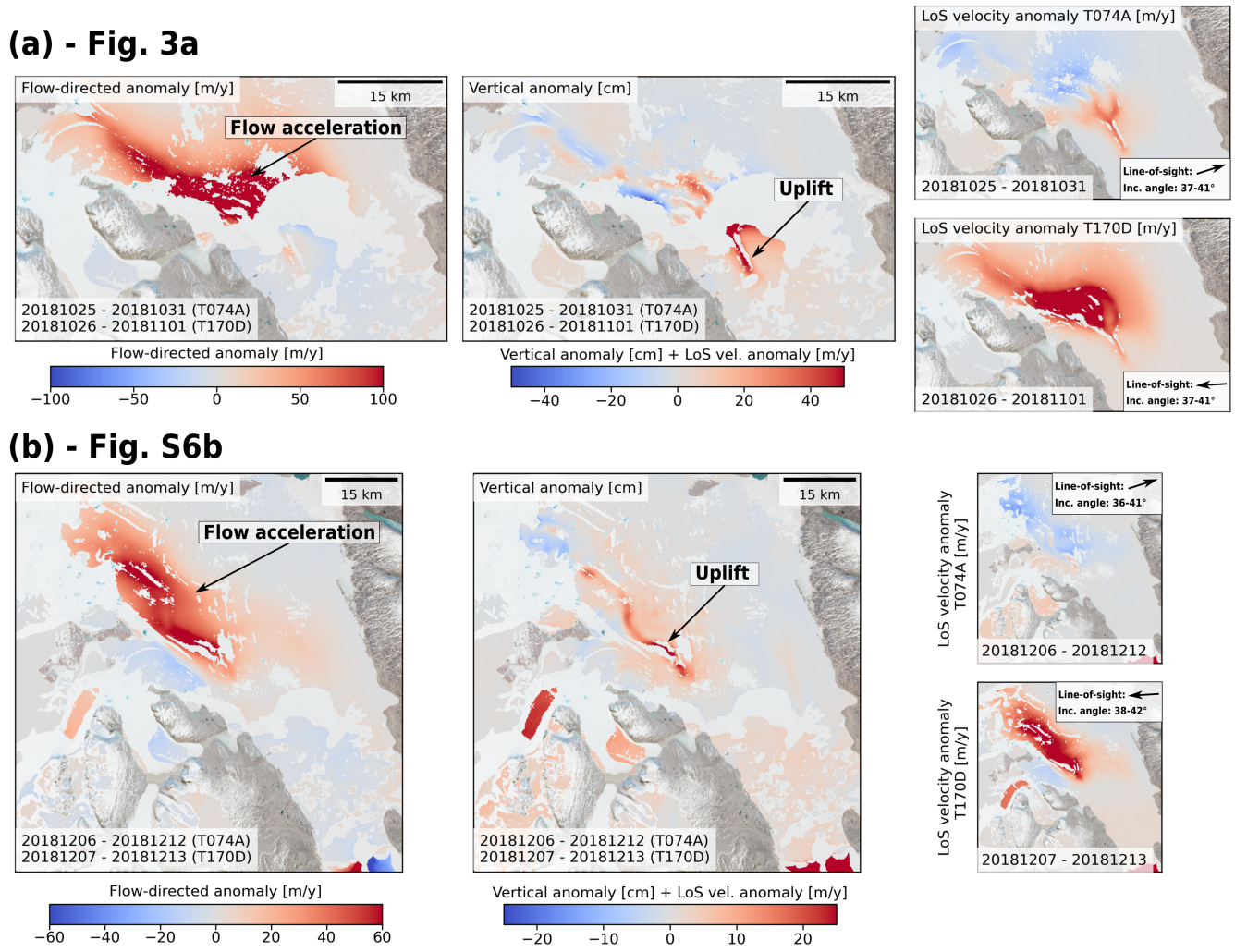


**Figure S2.** Evidence of flow acceleration and uplift following the October 2018 drainage presented in Fig. 3a-c (a) and the December 2018 drainage event presented in Fig. S6a-c (b). In each case, we show difference in line-of-sight (LoS) velocity for ascending track 74 (T074A) and descending track 170 (T170D) in the right-most panels, as well as the inferred differences in flow-directed (horizontal) velocity and vertical displacement. The differences are with respect to a pre-drainage event retrieval, that represents nominal flow (acquisition dates of these reference retrievals are provided in Table S1 below). Ground-projected LoS vectors and incidence angles are shown in the LoS velocity plots. The inversion to decompose flow-directed and vertical signals follows the approach outlined in Maier et al. (2023). The ice flow direction (assumed constant) is obtained from the 2016-2022 average 2D velocity mosaic from PROMICE. In case (a), we see both a high-magnitude flow speed-up (left-most panel) as well as an elongated uplift signal, which coincides with a subsidence signal measured $\sim 12$ days later (see Fig. S3a). The signals are somewhat obscured, because the decomposition is not possible in areas where ice flow direction approaches perpendicularity with the ground-projected line-of-sight direction of either of the tracks, leading to areas of missing data. A similar case is seen in (b) during the 2018 December drainage - superimposed on the flow speed-up signal is a channel-like feature of uplift, stretching about 30 km along flow.

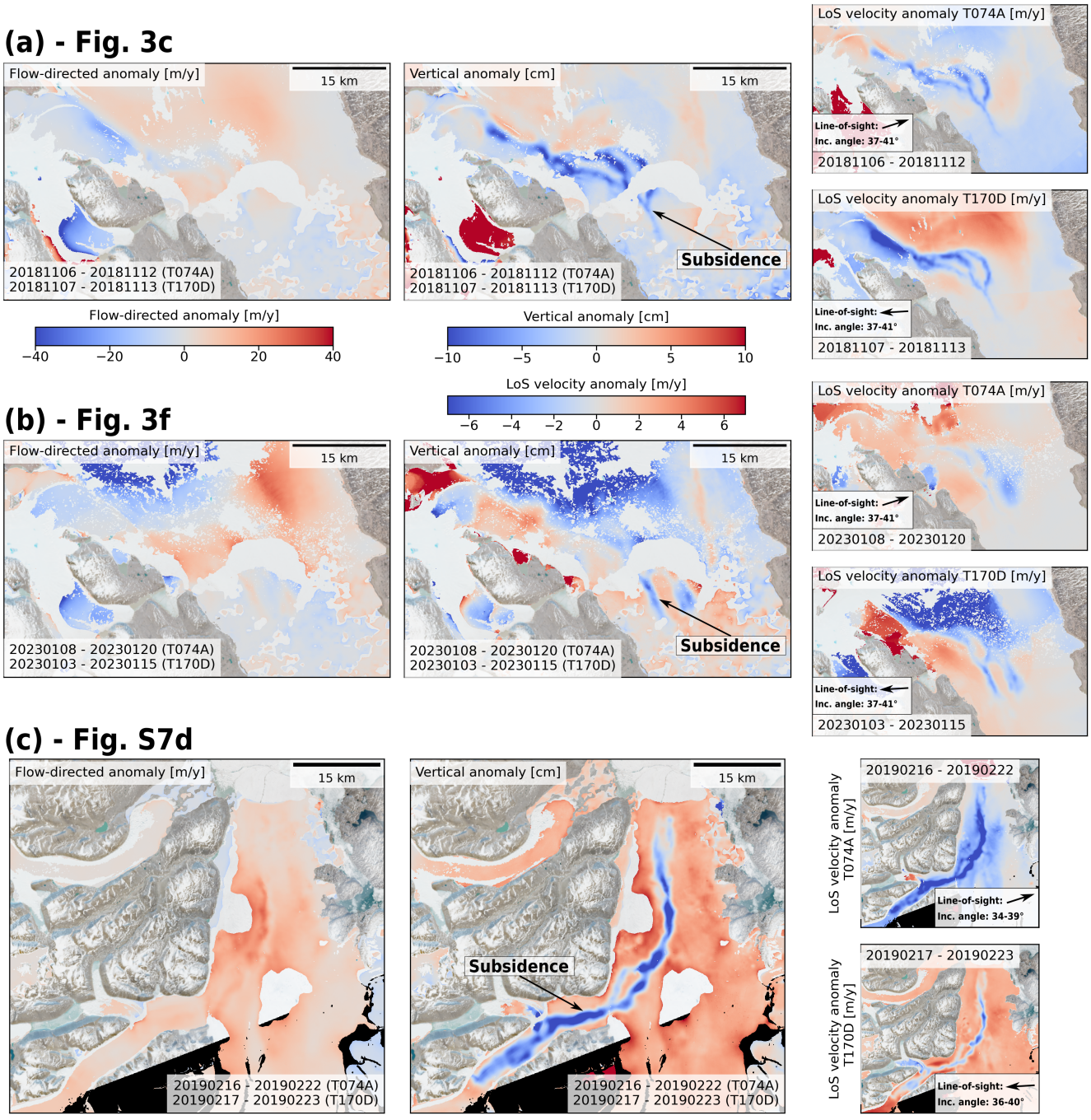


**Figure S3.** (Caption on next page).

**Figure S3.** (Previous page) Evidence of subsidence following the October 2018 drainage presented in Fig. 3a-c (a), the December 2022 drainage event presented in Fig. 3d-f (b), and the February 2019 drainage event presented in Fig. S7 (c). In each case, we show difference in line-of-sight (LoS) velocity for ascending track 74 (T074A) and descending track 170 (T170D) in the right-most panels, as well as the inferred differences in flow-directed (horizontal) velocity and vertical displacement. The differences are with respect to a pre-drainage event retrieval, that represents nominal flow (acquisition dates of these reference retrievals are provided in Table S1 below). Ground-projected LoS vectors and incidence angles are shown in the LoS velocity plots. The inversion to retrieve flow-directed and vertical signals follows the approach outlined in Maier et al. (2023). The ice flow direction (assumed constant) is obtained from the 2016-2022 average 2D velocity mosaic from PROMICE. In cases (a) and (c) we see distinct subsidence signals outlining bifurcating "channels". Case (b) is more problematic due to the increased temporal baseline of 12 days, increasing the difficulty of phase unwrapping, as well as the additional temporal separation between the image pairs (5.5 days, vs. 0.5 days for cases (a) and (c), meaning the two image pairs do not capture the same motion). Still, the LoS anomaly plots do show negative anomalies for both tracks that perfectly coincide with the downstream-most portion of the bifurcating channels observed in case (a), suggesting that these may be caused by subsidence (as negative anomalies indicate additional motion *away* from the sensor and the two tracks have opposite sensitivities to flow-directed motion in this region but near-equal sensitivities to vertical motion). Note that the inversion is not possible in areas where ice flow direction approaches perpendicularity with the ground-projected line-of-sight direction of either of the tracks (this includes part of the area in which subsidence is observed in cases (a) and (b)).

| Case | Reference (T074A) | Reference (T170D) |
|---|---|---|
| Fig. S2a | 20180919 - 20180925 | 20180920 - 20180926 |
| Fig. S2b | 20180919 - 20180925 | 20180920 - 20180926 |
| Fig. S3a | 20180919 - 20180925 | 20180920 - 20180926 |
| Fig. S3b | 20221109 - 20221121 | 20221116 - 20221128 |
| Fig. S3c | 20180919 - 20180925 | 20180920 - 20180926 |

**Table S1.** Acquisition dates of reference Sentinel-1 image pairs subtracted from the image pairs presented in Figs. S2 and S3.

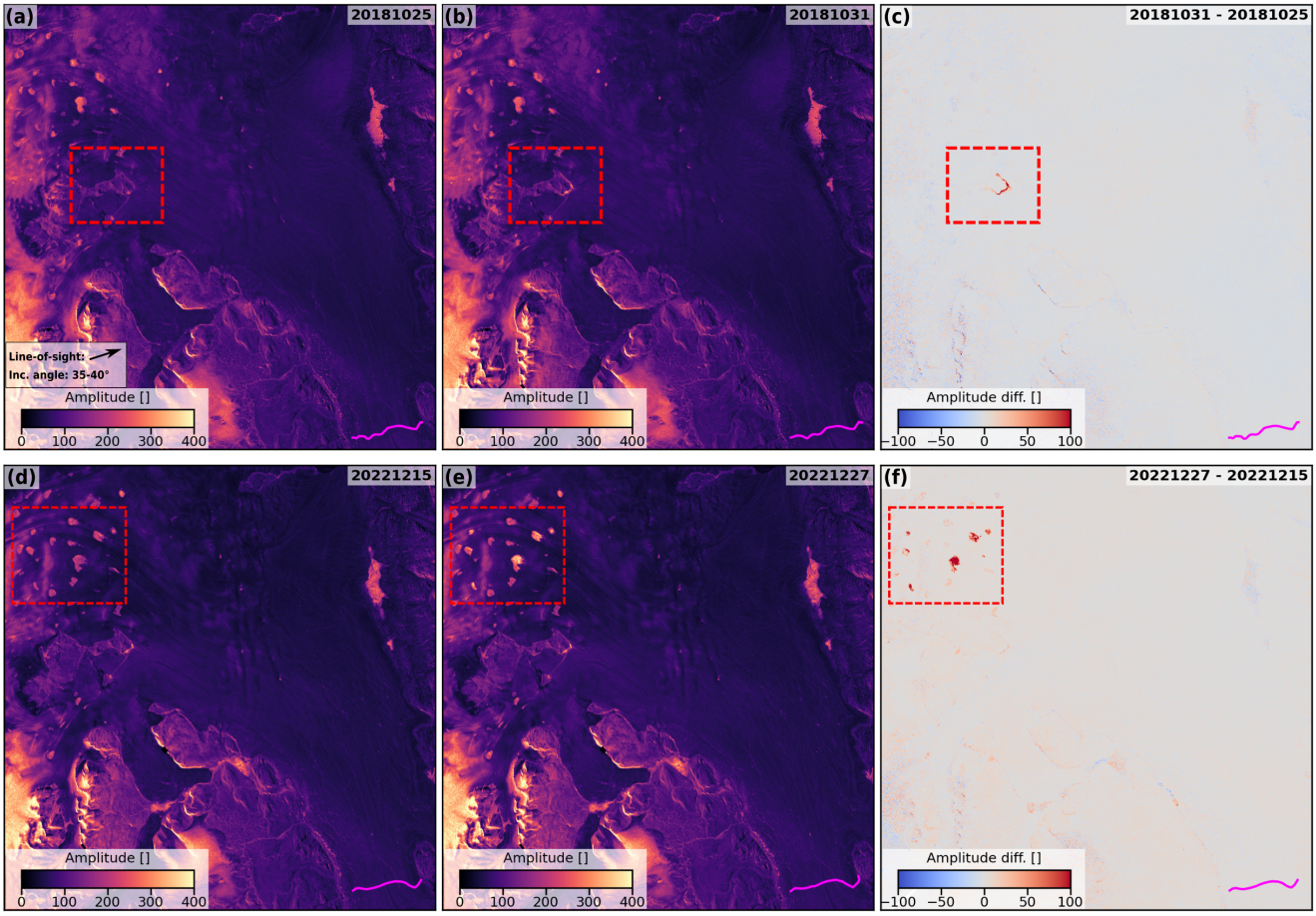


**Figure S4.** Sentinel-1 amplitude images revealing ice surface changes related to the transient dynamic events documented in Figure 3 in the main text. The imaged region is the same as in Figure 3. (a)-(b) Amplitude images from October 25th and 31st 2018 and (c) the amplitude difference between these acquisitions - an increase in amplitude is observed over an ice-dammed lake just upstream from where flow acceleration is observed (Figure 3 panels (a)-(c)), indicating a potential drainage of the lake. (d)-(e) Amplitude images from December 15th and 27th 2022 and (f) the difference between these acquisitions - amplitude increases are observed over multiple of the supraglacial lakes in this region, coinciding with the transient flow changes shown in Figure 3 panels (d)-(f), indicating that one or more of these lakes may have drained.

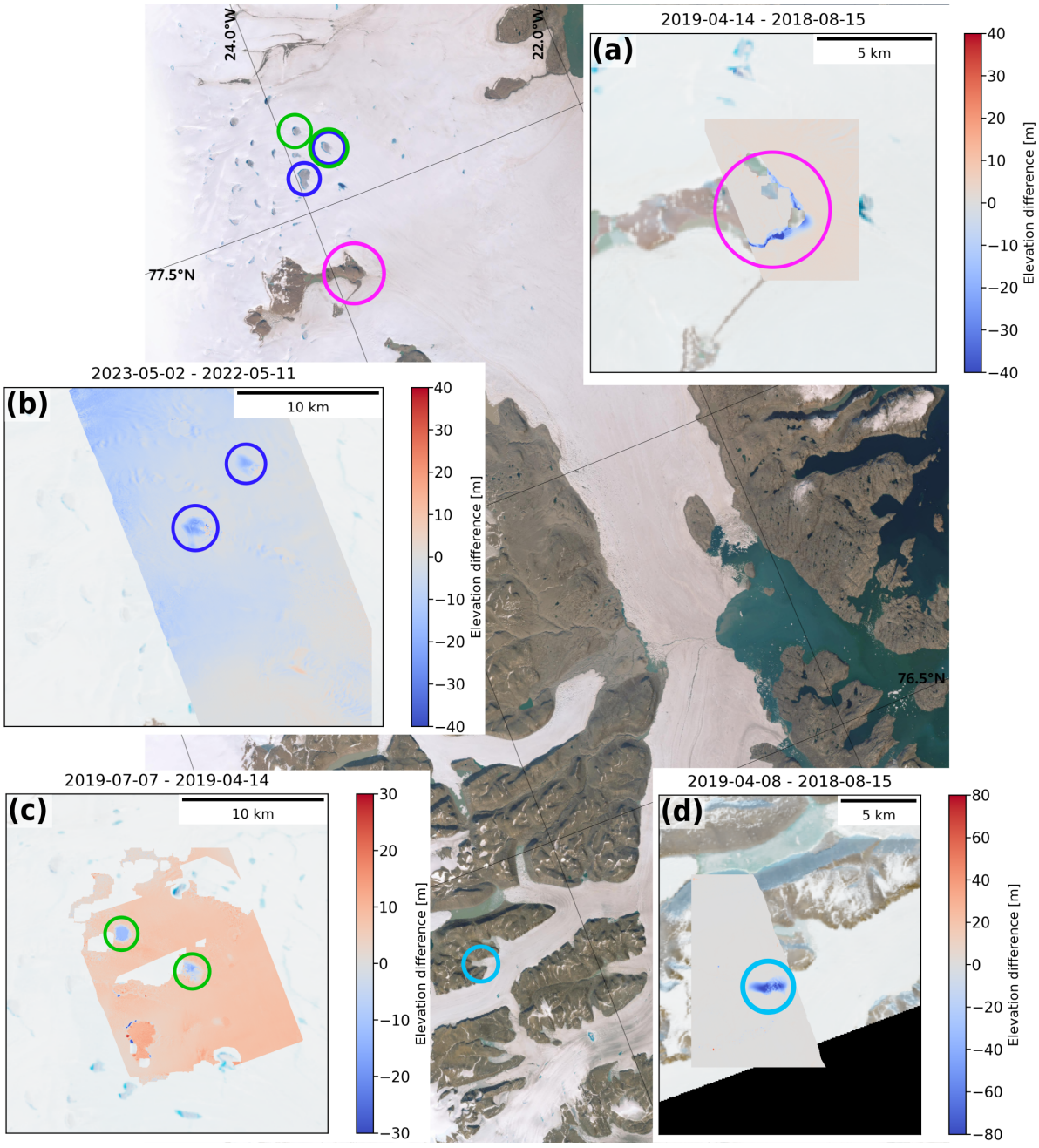


**Figure S5.** Elevation difference maps, generated by differencing ArcticDEM 2m strips from before/after the inferred drainage events. Colored circles show lake locations. (a) Elevation drop over an ice-dammed lake (see Figures 3a-c and S4a-c); (b) elevation drop over two supraglacial lakes (see Figures 3d-f and S4d-f); (c) elevation drop over two supraglacial lakes (see Figure S6d-f); (d) elevation drop over en ice-dammed lake (see Figures S7-S8). For the event identified in Figure S6a-c, we could not confidently identify a corresponding signal in the ArcticDEM measurements. The DEM difference maps were generated using the python tool *pdemtools* (Chudley and Howat, 2024), using the built-in coregistration function. In the cases of (b) and (c), limited to no bedrock is present in the strip, leading to a degraded coregistration, however, local anomalies are still observable over the lakes.

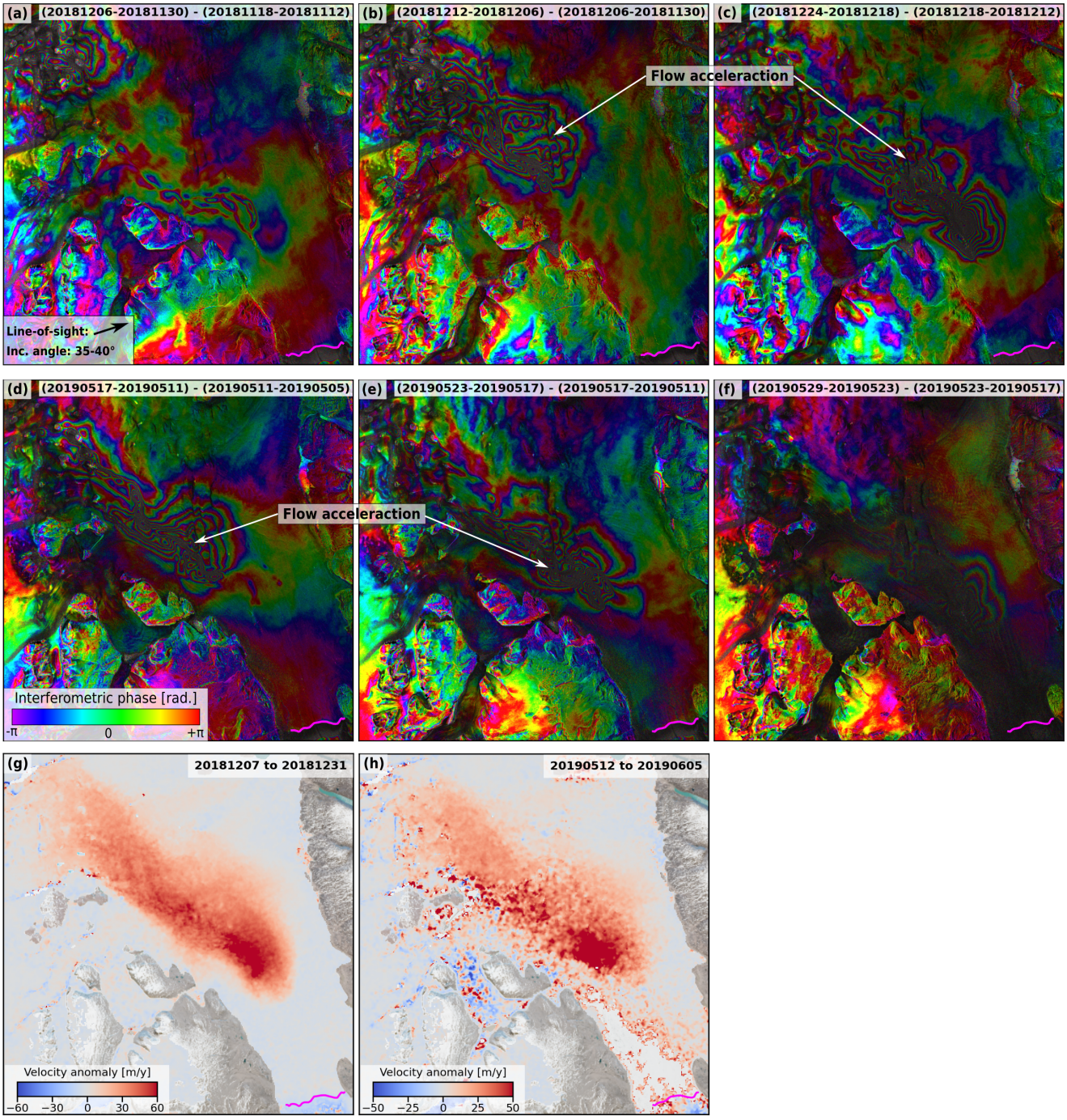


**Figure S6.** Sentinel-1 double-difference interferograms showing dynamical effects related to an apparent drainage event in upstream Storstrømmen during December 2018 (a)-(c) and May 2019 (d)-(f). The box in panel (a) indicates the ground-projected line-of-sight direction and incidence angle of Sentinel-1 track 74 (used for all the measurements in (a)-(f)). Panels (g) and (h) show PROMICE ice velocity magnitude anomalies for two 24-day periods spanning the identified events. The solid magenta line indicates the Storstrømmen grounding line.

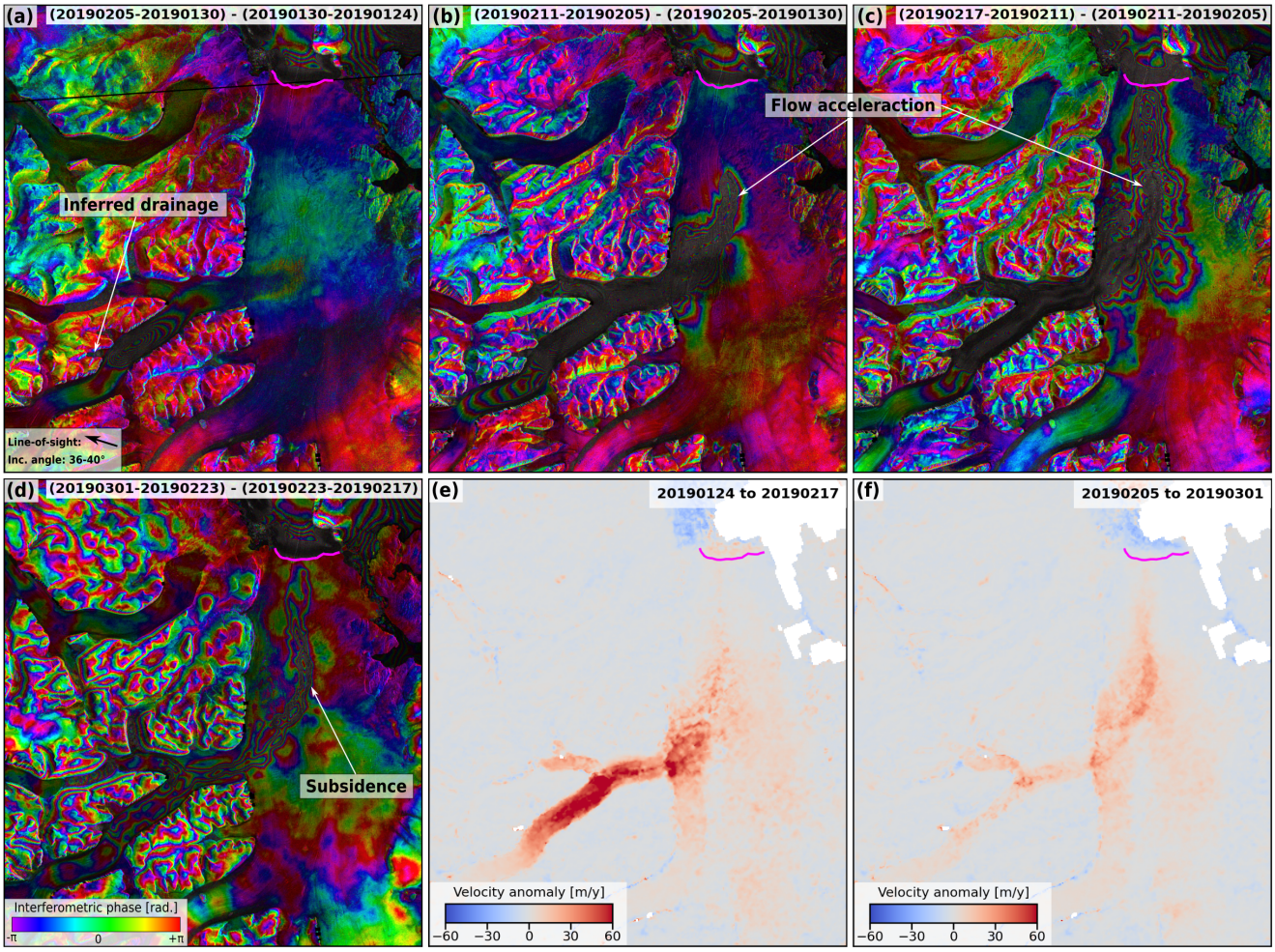


**Figure S7.** (a)-(d) Sentinel-1 double-difference interferograms showing dynamical effects related to an apparent drainage event upstream of L. Bistrup glacier during winter 2019. The box in panel (a) indicates the ground-projected line-of-sight direction and incidence angle of Sentinel-1 track 170 (used for all the measurements in (a)-(d)). Panels (e) and (f) show PROMICE ice velocity magnitude anomalies for two 24-day periods spanning the identified event. The solid magenta line indicates the L. Bistrup grounding line.

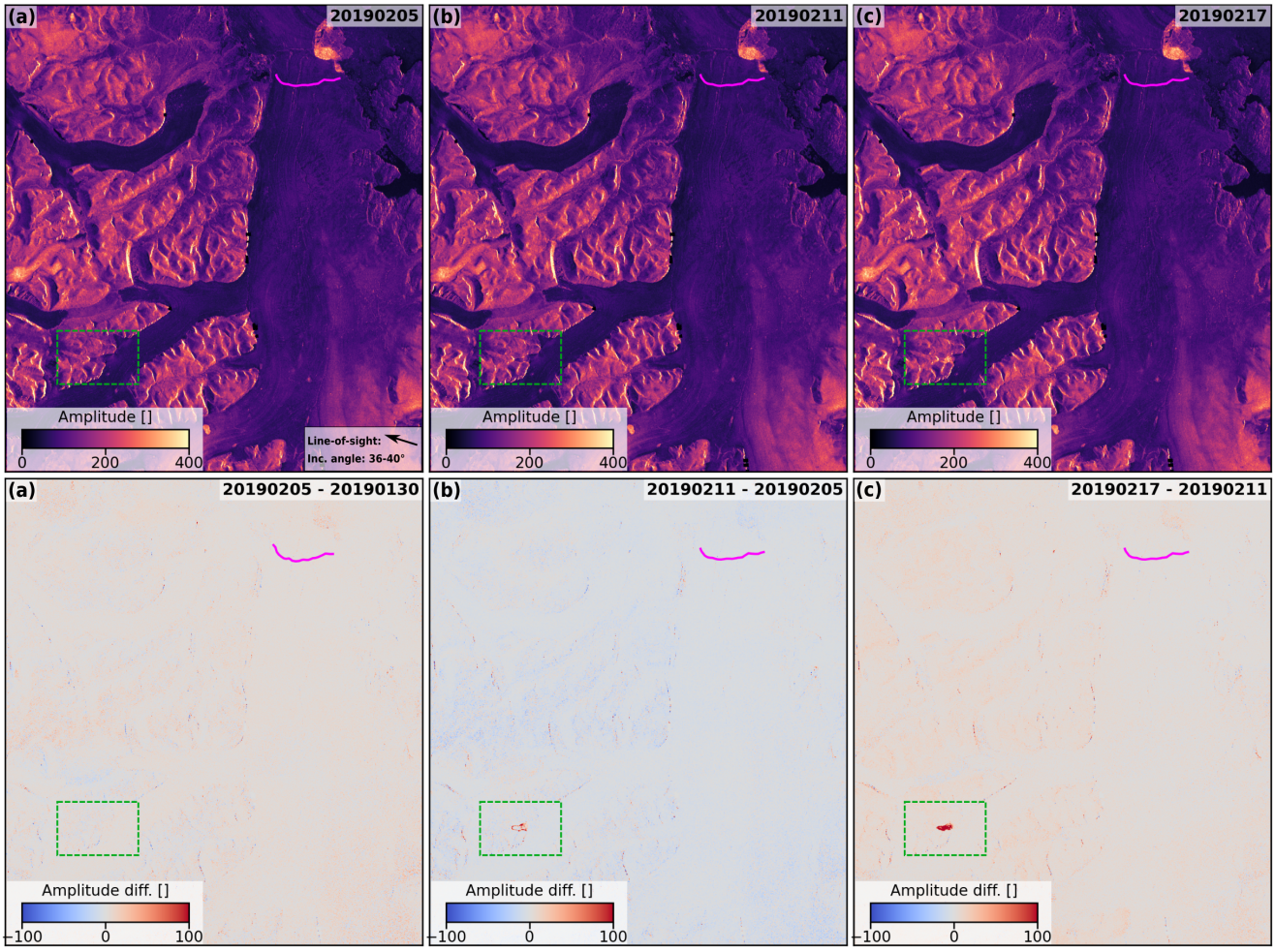


**Figure S8.** Sentinel-1 amplitude images revealing ice surface changes related to the transient dynamic events documented in Figure S7 above. (a)-(c) Amplitude images from February 5th, 11th, and 17th 2019. (d)-(f) Amplitude difference maps for these acquisitions - an increase in amplitude is observed over an ice-dammed lake just upstream from where flow acceleration is observed in Figure S7, suggesting a potential drainage of the lake (green dashed rectangle).

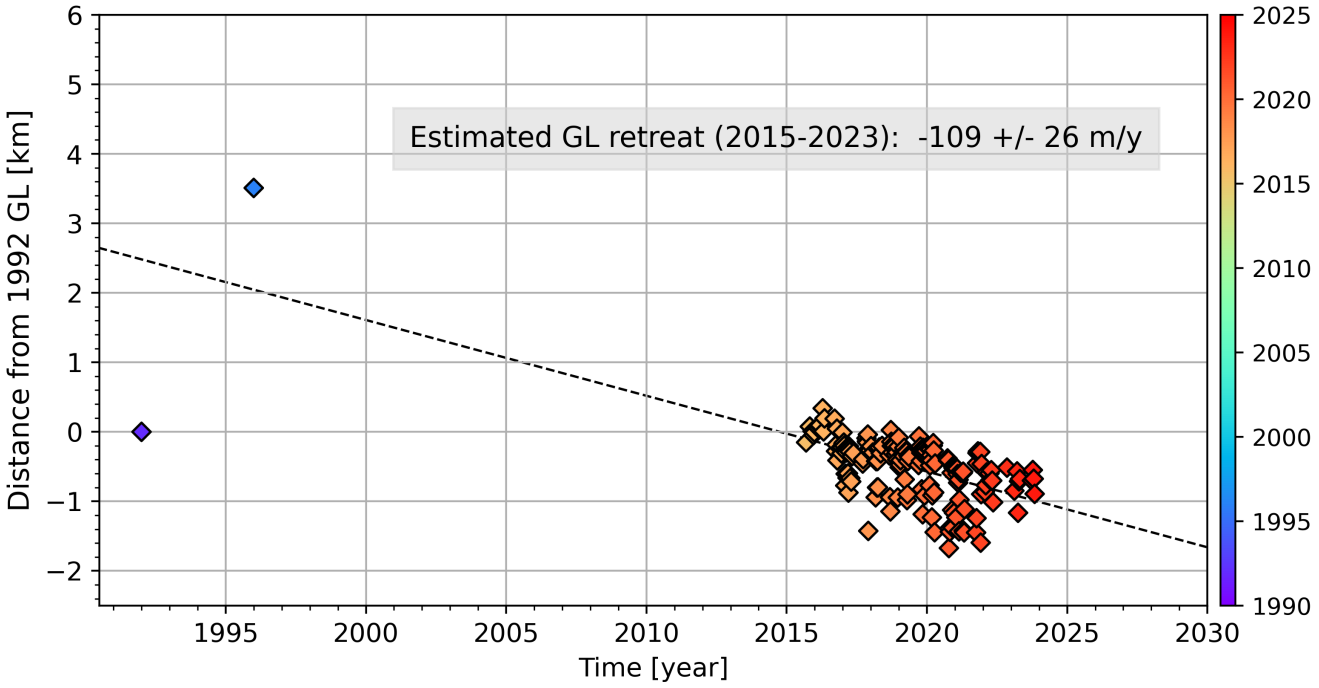


**Figure S9.** Time series of grounding line location for L. Bistrup (evaluated along the dashed transect in Figure 1). Grounding line locations are measured with double-difference interferometry using images from Sentinel-1 (2015-2024) and ERS-1/2 (1992-1996, data obtained from Mouginot et al. (2018)). Note that we exclude the 1992-1996 measurements from the linear fit, as L. Bistrup underwent a surge during this time. The short-term variability of the grounding line location is much higher for L. Bistrup than for Storstrømmen: the standard deviation of the de-trended grounding line location (excluding 1992-1996 data) is 338 m for L. Bistrup, compared to 119 m for Storstrømmen (see also Figure 1c in the main text for comparison).